Alternation of asphaltene binding arrangement in the presence of chemical inhibitors: Molecular dynamics simulation strategy

Ghamartale Ali, Rezaei Nima, Zendehboudi Sohrab

DOI: 10.1016/j.fuel.2022.127001

Alternation of asphaltene binding arrangement in the presence of chemical inhibitors: Molecular dynamics simulation strategy

Ali Ghamartale[1], Nima Rezaei[1,2], Sohrab Zendehboudi[1*]

[1]Department of Process Engineering, Memorial University, St. John's, NL, Canada
[2]Department of Separation Science, Lappeenranta-Lahti University of Technology, Finland
Email Address of Corresponding Author: szendehboudi@mun.ca

Asphaltene deposition is one of the challenging issues in petroleum production and transportation. Chemical inhibitors are commonly employed to postpone the asphaltene aggregation, which is the primary stage of asphaltene deposition. Design and introduction of an effective chemical inhibitor have always been a challenge for the industry, considering substantial variations in characteristics and structures of asphaltene and petroleum. The binding arrangement of asphaltene is a factor of aggregate stability, which depends on asphaltene structures. This feature alters in the presence of chemical inhibitors. In this work, molecular dynamics (MD) simulation is employed as a cost-effective and accurate method to study the impact of chemical inhibitors on the binding arrangement of two asphaltene structures. One asphaltene structure has a hydroxyl group and pyridinic nitrogen in its polyaromatic core, while another lacks both groups. The chemical inhibitors are octylphenol (OP), 1-butyl-3-methylimidazolium bromide ([BMIM][Br]), and 1-butyl-3-methylimidazolium chloride ([BMIM][Cl]). The simulation results show OP cannot stop the quadrupole-quadrupole interaction between the asphaltenes since the force between OP's benzene ring and asphaltene polyaromatic core is weaker than the force between two polyaromatic cores. Nevertheless, OP forms a hydrogen bond with the asphaltene and prevents asphaltene molecules from approaching each other by providing steric hindrance around the molecules. As a result, OP does not show a promising potential to reduce the parallel stacking, especially for the asphaltene with no hydrogen bond potential, while it relatively reduces the T-shape arrangement for both asphaltenes. The ionic liquids (ILs) beat the quadrupole-quadrupole interaction between the asphaltene cores with cation-quadrupole force and notably reduce the parallel stacking. They also lower the number of T-shape binding arrangement between the asphaltene molecules. The shape and binding arrangement of polyaromatic compounds (such as asphaltene) are not only important in the petroleum industry but also these features play a crucial role in designing optical and electronic nanodevices. The introduced approach is a new pathway to improve the design of chemical inhibitors that affects the aggregation arrangement of polyaromatic compounds.

Keywords: Continental asphaltene; Chemical inhibitors; Ionic liquids; Binding interaction; Molecular dynamics simulation

1. INTRODUCTION

Resins can stabilize the asphaltene molecules in crude oils; however, changes in the thermodynamic conditions can destabilize the asphaltenes, resulting in asphaltene aggregation. The aggregate formation disrupts oil production and transport by changing the fluid properties such as solubility, density, and viscosity [1]. Chemical inhibitors are commonly added to crude oil to improve the asphaltene suspension stability and avoid asphaltene aggregation [2, 3]. Chemical inhibitors are used in the oil industry for decades; however, designing and synthesizing an efficient inhibitor for a target crude oil have always been challenging. Self- and cross-association energies between the asphaltene and inhibitor molecules

are critical design parameters when choosing an inhibitor for given crude oil and reservoir properties. Although the π-π stacking is considered one of the main mechanisms for asphaltene binding [4], other driving forces and mechanisms are also hypothesized for the asphaltene binding for different asphaltene chemical structures and crude oil compositions [5, 6]. Various functional groups such as hydroxyl and carboxyl are presnet in the chemical structure of asphaltene. Therefore, the asphaltene binding behavior is affected by various types of interactions, including van der Waals, Coulombic, exchange-repulsion interactions, and induction forces (such as hydrogen bond and π-π stacking) [1, 7]. Adequate understanding of the asphaltene binding with itself and with the inhibitor molecules is imperative for designing chemical inhibitors to prevent asphaltene aggregation. Chemical inhibitors usually bind to the asphaltene molecules, providing steric hindrance and disrupting the asphaltene self-interaction [8].

The asphaltene binding arrangement is a quantitative measure of the aggregate formation potential [9] that depends on the number of aromatic rings in the polyaromatic core [4]; the type and number of functional groups [10]; the type, number, and location of heteroatoms [4, 11]; and the length, number, and location of alkyl chains [6]. For instance, asphaltenes with a larger aromatic core, or with nitrogen atoms in their aromatic cores (e.g. pyridinic form), have a higher self-aggregation tendency [4], while sulfur atoms in the asphaltene aromatic core reduce the asphaltene self-aggregation due to steric hindrance and Coulomb repulsion [11]. There are three main arrangements proposed for the asphaltene aggregation: face-to-face (also called parallel stacked or π-π stacked), offset stacked (offset parallel stacked, offset π-stacked, or parallel displaced), and T-shape (π-σ stacked, perpendicular stacked, or edge-on stacked) [12-14]. The number of aromatic rings in the asphaltene polyaromatic core plays a major role in the asphaltene binding arrangement [6]. For instance, molecules containing a single aromatic ring, such as benzene, form T-shape bonding to minimize the repulsion force [15, 16]. In contrast, asphaltene molecules with multiple aromatic rings such as asphaltenes bind preferentially through parallel arrangements [12, 17-19], including the face-to-face [17] and offset stacked [12, 18, 20]. Arrangements different than the parallel types are packed much looser and have an irregular outward form, which greatly impacts the final aggregate shape [21].

Molecular dynamics (MD) simulation has been used to understand the asphaltene binding arrangements and to analyze the influence of various parameters, including aromatic core size [4], functional groups [22], heteroatoms position [11], side chain (lengths and number) [4, 6, 23], solvent properties [24-26], and thermodynamic conditions [12, 19]. In the previous studies, the asphaltene behavior was investigated in the bulk phase [1, 4, 6, 10, 11, 19, 23, 24, 27] and the water-oil interface [10, 22, 28-32]. In the following, we review the MD studies to analyze the asphaltene binding arrangements. Zhang and Greenfield [19] were the first researchers to investigate the angle between asphaltene molecules (in an aggregate) to measure the asphaltene binding arrangement for two different asphaltene chemical structures. They used an asphaltene structure with a small aromatic core and long side chains, and another one with a large aromatic structure and short side chains. The asphaltene with a small aromatic core formed parallel arrangements at high temperatures and perpendicular at low temperatures, while the asphaltene with the large aromatic core demonstrated opposite behavior with temperature [19]. Sedghi et al. [4] adopted different asphaltene structures and studied the asphaltene arrangements in the dimerization process. They considered the potential mean force versus distances between two asphaltene molecules to analyze the binding arrangements. Potential mean force curves showed a drop at 0.5 nm for all asphaltene structures, which represented the offset parallel stacking. The T-shape dimerization arrangement was explained by observing a minimum at 0.7–0.8 nm in the potential mean force curves for various asphaltene structures, although the T-shape arrangement vanished for asphaltene structures

with side chains. Jian et al. [6] used the minimum distance and angle between asphaltenes to study the effect of side-chain size on the aggregation mechanisms in water. The Violanthrone-78 asphaltene with 16, 12, 8 and 4 carbons alkyl side chains were tested. The asphaltene with the side chain length of 4- and 16-carbon had a similar aggregation intensity and trend but through different mechanisms. They claimed that polyaromatic core stacking is the dominant aggregation mechanism for the asphaltene with a short side chain. However, the alkyl side chains interacted with themselves for the asphaltene structure having a long side chain, and resulted in a similar aggregation rate. The T-shape arrangement was observed at equilibrium stage and produced rod-like aggregates [6]. Jian and Tang [24] studied the importance of asphaltene medium properties on asphaltene aggregate shape and arrangement by considering water, toluene, and *n*-heptane as bulk fluid. In water, polyaromatic compounds minimized the contact with water, and the aggregates were spherical. Using *n*-heptane, its molecules interacted with the asphaltene side chains and minimized the interactions between the polyaromatic cores and side chains. Therefore, parallel stacking was considered as the dominant aggregation mechanism and led to large rod-shape aggregates. Using toluene, the parallel stacking was also dominant; however, the aggregates were smaller than those in *n*-heptane [24]. Takanohashi et al. [33, 34] also noted the importance of bulk fluid by studying the dissociation of coal molecules in benzene, methanol, and pyridine. Pyridine was an effective fluid for dissociating asphaltene aggregates because it could form both hydrogen bonds and parallel stacking. Gao et al. [10] compared the aggregation arrangements of an asphaltene with a carboxyl group and an asphaltene with a carboxylate group in crude oil through an MD simulation. The first asphaltene was more prone to form face-to-face aggregates, while the second asphaltene had both face-to-face and T-shape arrangements. They also confirmed the argument by the quantum mechanics simulation. Sodero et al. [11] used the minimum distance and the angle between the asphaltene molecules to probe the effect of heteroatom location on asphaltene aggregation. They found parallel stacking to be the main aggregation mechanism; the location of the heteroatoms in the asphaltene molecule affected the strength of the binding interaction. For instance, the presence of sulfur atoms in an asphaltene core reduced the asphaltene parallel stacking, while the presence of a sulfur atom in the asphaltene alkyl branch enhanced the aggregate stability due to interaction with the carboxylic group [11]. Wang et al. [23] studied the effect of length and number of side chains on the most plausible aggregation arrangement for asphaltene with 5 to 8 aromatic rings under vacuum environment. They concluded that asphaltene chemical structures with short or no side branches prefer face-to-face stacking as the dominant aggregation arrangement, while the long side branch led to a mixture of parallel stacking and T-shape arrangements. Teklebrhan et al. [1] used a similar analysis and studied the asphaltene aggregation when naphthenic acid was present in asphaltene-toluene mixture. The naphthenic acid restricted the formation of hydrogen bonding between the asphaltenes and forced asphaltenes to form longer parallel stacking. Shorter naphthenic acids restricted the asphaltene self-aggregation (through hydrogen bonds) more than longer ones [1]. Table 1 present a summary of recent studies on asphaltene binding arrangements.

Table 1. Summary of recent studies on asphaltene binding arrangements

Number of Asphaltene types* (vary in)	Space	T [K] / P [bar]	Software (forcefield)	Ensemble (sampling time [ns])	Remarks	Ref
2 (side chains)	Naphtalenes/ saturates mix	238.15-443.15 / -	LAMMPS (OPLS-AA)	NPT (3)	A small polyaromatic core causes parallel stacking (at high T) and perpendicular pattern (at low T), oppositely than asphaltene with a large polyaromatic core.	[19]
8 (side chains and functional groups)		300 / (1)	GROMCAS (OPLS-AA)			[4]

	Vacume, heptane & toluene	1		Umbrella sampling (10)	Asphaltene with no side chain forms both offset parallel and T-shape while side chains prevent T-shape arrangement.	
4 (side chains' size)	Water	300 1	GROMACS (GROMOSE)	NPT (60)	Parallel stacking is dominant for asphaltene with short side chains. While long alkyl side chains interact and change binding patterns.	[6]
4 (side chains' size)	Heptane, toluene & water	300 1	GROMACS (GROMOSE)	NPT (180)	Asphaltenes have minimum contact with water, and form a spherical shape. *n*-heptane and toluene interact with side chains, and parallel stacking becomes dominant.	[24]
2 (functional groups)	SAR mixture	298 1	GROMACS (GROMOSE)	NVT (200)	The carboxyl asphaltene forms face-to-face binding, while the carboxylate asphaltene forms face-to-face and T-shape arrangements.	[10]
4 (sulfur location)	Toluene	298 1	GROMACS (GROMOSE)	NPT (20)	4 sulfurs in the aromatic core reduce parallel stacking due to Coulomb repulsion. Sulfur in side chains impacts binding stability due to interacting with oxygens and hydrogens.	[11]
1	Toluene	298 1	GROMACS (GROMOSE)	NPT (50)	Naphthenic acids reduce the hydrogen bonding between asphaltenes and result in parallel stacking enhancement.	[1]
11 (side chains' size)	No solvent	300 -	Amber (UFF & Amber)	- (0.5-1000)	Small side chains result in severy ordered parallel stacking. Parallel stacking disorder and vanish by increasing side chain length.	[23]
20 (core size and lateral chain size)	Toluene	298-423 1-15	GROMACS (GROMOSE)	NPT (60)	Parallel stacking is the only pattern when the number of aromatic carbon exceeds 29. The length of side chains controls nanoaggregate numbers and does not prevent π-stacking.	[33]
6 (side chains' size and number)	No solvent & toluene	300 & 535 1	LAMMPS (PCFF)	NPT (150-250)	Several alkyl side chains result in "phase separated columnar" structure. While "separated lamellar" structure is observed for two symmetry alkyl side chains.	[34]
20 (side chains' size and number)	Toluene	298.15 1	GROMACS (Amber)	NPT (10-20)	Asphaltenes disaggregate easier due to steric hindrance of side-chains and T-shape dispersion attraction.	[35]
2 continental & 1 archipelago	Water	298-498 50	Material Studio (CAMPASS)	NPT (30)	SDBS, unlike SDS, causes higher parallel stacking and T-shape for asphaltene-surfactant interaction due to having a benzene ring.	[36]
15 (heteroatom in the core and lateral chain number)	(chloro-, bromo- & isopropylen) benzene, toluene & benzene	298 1	Material Studio (CAMPASS)	NPT (1)	Face-to-face stacking is dominant in the absence of solvent, while phenols and isopropylene benzene interrupt that. Increasing the length of asphaltene side chains prevents cores' proximity.	[37]
1	Quinoline, toluene, & ethanol	298.15 1	Material Studio (CAMPASS)	NPT (1.5)	Attraction energy for parallel stacking is higher than hydrogen bonding. Both quinoline and toluene interrupt parallel stacking, while ethanol impact hydrogen bonding.	[38]
1	SAR mixture	323 -	GROMACS (Amber)	NPT (60)	Viscosity reducer agents change the face-to-face arrangement between asphaltenes to a weaker face-to-face and T-shape arrangement between asphaltene and resins.	[39]
2	SAR mixture	300 1	GROMACS (GROMOSE)	NPT (50 ns)	Asphaltene forms parallel stacking and T-shape with asphaltenes and resins. Surfactants weaken and prevent stacking.	[40]

*All asphaltene types are continental except one study [36] that is mentioned.

Despite the strong interest to develop (and introduce) a reliable inhibitor, there is no systematic research to study the asphaltene binding arrangement with an asphaltene inhibitor and to elaborate on the asphaltene aggregation mechanisms and asphaltene-inhibitor interactions. Lack of molecular knowledge on the binding arrangements and intermolecular network formation between the asphaltenes and inhibitors limits the design and preparation of chemical inhibitors. In this study, we use radial distribution function, the aggregate shape index, and the angle and distance between the molecules to explore the asphaltene binding arrangement manipulation by different inhibitors. We also improve the criteria to distinguish various types of asphaltene binding arrangements. To achieve these objectives, two different continental-type asphaltene structures with and without functional groups are considered using of three different inhibitors. For the inhibitors, we use a surfactant, *n*-octylphenol (OP), and two ionic liquids (ILs), 1-butyl-3-methylimidazolium bromide ([BMIM][Br]), and 1-butyl-3-methylimidazolium chloride ([BMIM][Cl]). We also use *n*-heptane as a precipitant.

The paper is structured as follows: after the introduction, the methodology and the analysis methods are elaborated in detail in Section 2. Also, in section, we propose our novel method to distinguish between types of asphaltene binding arrangements. Section 3 starts with validating our result by comparing the density parameter and then proves the repeatability of simulation runs. This section also discusses chemical inhibitors' impact on the asphaltene binding arrangement types. The last part is dedicated to concluding remarks. The highlighted results of this paper help to further understand the molecular interactions between asphaltene and asphaltene-inhibitor and provide valuable guidance for future inhibitor design.

2. METHODOLOGY

2.1. Simulation and Modeling Framework

Molecular scale simulation is divided into three main categories: molecular mechanics, quantum mechanics, and molecular dynamics (MD). Among them, MD measures the parameter dynamically, while the other two methods have no time dimension. In MD the molecular movement is based on solving the second Newton's law. Molecular mechanics and quantum mechanics are based on solving the Schrödinger equation which is computationally more demanding. This significantly limits the number of atoms in the system and necessitates large CPU/GPU resources for the two latter methods. Another difference is the molecule structures, and covalent bonds are usually fixed in MD, while the other two methods are specifically useful when the covalent bond changes, or when the chemicals reacts. MD is a beneficial tool in chemistry, biochemical, and drug discovery research to probe mechanisms. MD applications have been recently expanded into engineering and petroleum research with a mechanistic approach. We employ the MD method in this study using the GROMACS software [41, 42]. Based on our previous research, we use the OPLS-AA forcefield due to its accuracy in calculating the thermodynamic properties of hydrocarbons such as benzene [43].

There is a debate whether the continental or archipelago asphaltenestructures are the most dominant representatives. Mikami et al. [28] simulated three types of asphaltenes: continental, archipelago, and resin. They compared the properties of the oil generated from the simulation with experiments and theoretical studies and confirmed that the simulation with continental type could predict the oil properties more accurately compared with experimental and theoretical results. In 2017, Wang et al. [23] summarized experimental studies and suggested the continental asphaltene structure as the main and dominant structure. Also, we studied the aggregation of an archipelago asphaltene with and without

inhibitors in *n*-heptane, and we did not observe a severe aggregation for the archipelago-type asphaltene even in the absence of inhibitors [44]. Therefore, we consider two continental asphaltene structures, used in our previous study [44], as shown in Figure 1(a)–(b), to study the potential effects of hydrogen bonds in the presence of chemical inhibitors. Literature shows that octylphenol, nonylphenol, and ethoxylated nonylphenol are effective surfactants to inhibit asphaltene aggregation, while the ionic liquids are newer inhibitors that are more environmentally friendly [45, 46]. Therefore we adopted octylphenol (OP), 1-butyl-3-methylimidazolium bromide ([BMIM][Br]), and 1-butyl-3-methylimidazolium chloride ([BMIM][Cl]), as depicted in Figure 1(c) as inhibitor of asphaltene aggregation for further investigation.

The structures are built with Avogadro software [47] and optimized with Gaussian09 software, using 6-31g(d,p) basis set. Four boxes of *n*-heptane (nC_7) with an initial dimension of $(15)^3$ nm^3 are made for each asphaltene type. The box size reduces when the pressure and temperature are adjusted to reach the right volume. The box dimensions at the end of the simulation are in the range $(10.65)^3 – (10.75)^3$ nm^3 for various cases, depending on the components to reach the correct density at the target temperature and pressure. A total of 50 asphaltene molecules (with 7 wt % concentration) are distributed in each of the nC_7 boxes. One box is simulated with no additives as a control system, while in each of the other three boxes, 7 wt% of one inhibitor is added. The number of the inhibitor molecules is 177 for OP, 167 for [BMIM][Br], and 209 for [BMIM][Cl] [44].

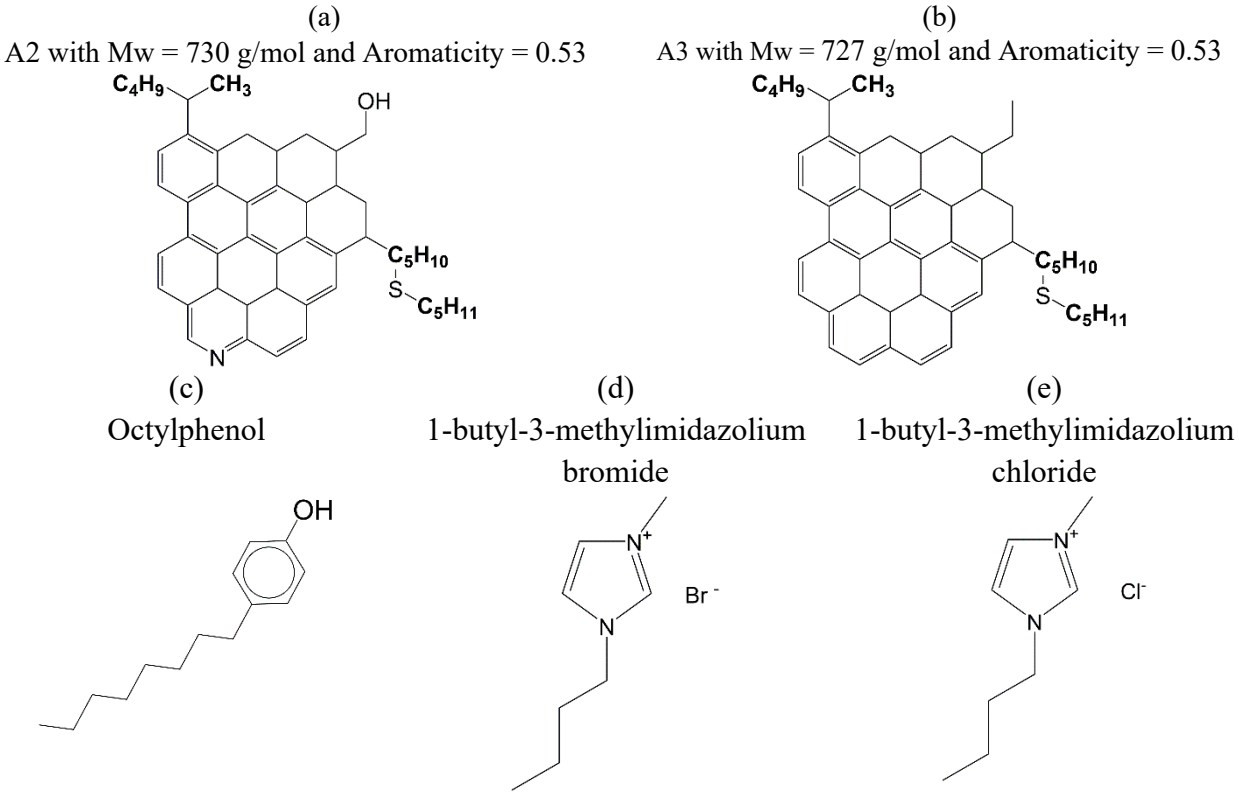

Figure 1: The chemical structures of: (a) A2 continental-type asphaltene with the potential to form hydrogen bonds; (b) A3 continental-type asphaltene with no potential to form hydrogen bonds; (c) surfactant inhibitor: octylphenol ; (d) ionic liquid inihibitor: 1-butyl-3-methylimidazolium bromide; (e) ionic liquid inhibitor: 1-butyl-3-methylimidazolium chloride.

The simulation algorithm involves four steps. The first step includes the minimization of system energy by avoiding overlapping molecules or very close positioning between the atoms in the initial

configuration. The steepest descent method is applied for energy minimization. In the following, the system temperature adjusts to 300 K by running the NVT simulation for 100 ps. The velocity rescaling thermostat is considered for the NVT simulation. In the third step, the pressure adjusts to 1 bar at the pre-adjusted temperature by running the NPT simulation for 1 ns. The density changes are shown for the case of A2/nC$_7$ as an example in Figure 2 to demonstrate that our systems have reached equilibrium after adjusting the pressure and temperature for 1 ns. The velocity rescaling thermostat and the Berendsen barostat are considered in the NPT simulation. The last step is data sampling at the target temperature and pressure (300 K and 1 bar), by running the simulation for 120 ns. The Nose-Hoover thermostat [48, 49] and the Parrinello-Rahman barostat [50] are employed for the data sampling. In the sampling step, the positions of molecules are recorded every 10 ps and used in the post-analysis. More details about the simulation framework can be found in our previous work [44].

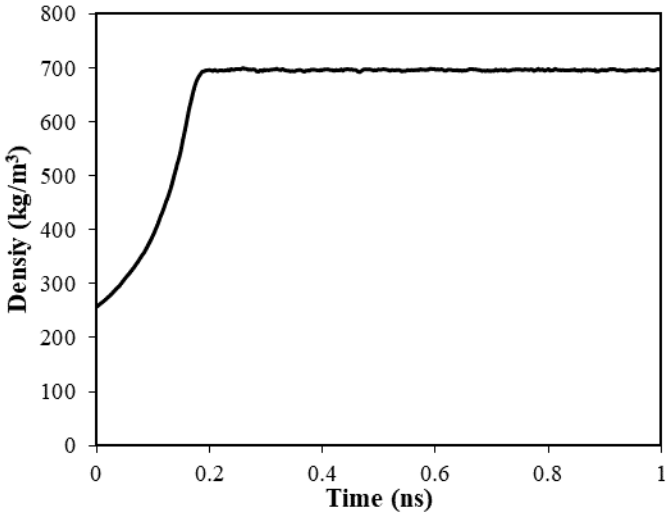

Figure 2. Density changes for the A2/nC$_7$ box during the NPT ensemble, pre-equilibrium stage.

2.2. Analysis Methods

Radial distribution function (RDF): The RDF or $g(r)$ shows the probability of observing two types of molecules within a distance over the adjusted period, and identifies the intensity of molecules' binary interactions. In this study, the RDF is calculated between the centre-of-mass (COM) for asphaltene molecules in the final 60 ns of the simulation using the trajectory file. This analysis is conducted with a built-in tool in GROMACS, *gmx rdf*.

Aggregate Shape: The asphaltene non-covalence bond cause the asphaltene aggregates with various shapes during the simulation; we use asphericity index is used to analyze the aggregate shapes. The asphericity index varies between zero and one. The asphericity index of zero corresponds to a sphere and as the index approaches one, the aggregates become rod-like [44]. In this study, the average asphericity index for the aggregates in each frame is determined, and its probability density is plotted in the final 60 ns of simulation. MDAnalysis package in Python is employed to conduct this analysis [44].

Angle-distance analysis: Commonly, asphaltene pairs with a distance < 0.5 nm are classified as the face-to-face stacked aggregates in the literature; those with a distance between 0.5 to 0.75 nm are considered as the offset stacked; and those with a larger distance up to 1.5 nm are considered as the T-shape [6, 10,

30, 32, 51]. However, Jian and Tang [24] showed that asphaltenes could form the parallel arrangement at a pair distance of 0.45, 0.75, 1.1, and 1.5 nm, which was also confirmed by Teklebrhan el al. [1]. Therefore, classifying the asphaltene aggregate mechanisms solely based on the pair distance can be inconclusive. For an accurate classification, both the angle and distance criteria should be considered. In this study, the distance between the COM of asphaltene molecules is measured using *gmx distance*, a built-in tool in GROMACS. The angle between two asphaltenes' polyaromatic cores is calculated using *gmx gangle* by measuring the angle between the polyaromatic planes. The aromatic plane is defined by considering a plane connecting three carbon atoms in the asphaltene core, shown by orange dots in Figure 3. The angle between two planes, shown with grey diamonds, is measured by the angle between the normal vectors to the planes (Figure 4 (a)). If the normals of planes are concurrent (n_1 and n_2), the θ-angle is between 0 º and 90 º; if they are counter-current (n_1 and n_2'), the θ-angle is in the range of 90 º – 180 º (Figure 4(b)). In this study, the θ-angle is assigned to distinguish the T-shape arrangement from the face-to-face and offset stacking. For the angle 60 º < θ < 120 º, the T-shape arrangement is considered for asphaltene binding, and for θ < 30 º or θ > 150 º, the parallel stacked (either face-to-face or offset stacked) arrangement is considered. To differentiate between the face-to-face and offset arrangements, we employ α-angle between a vector which connects the center of two planes, $\overrightarrow{AB}$, and the resultant vector of plane normals ($\vec{R}$), as depicted in Figure 4 (c). The $\vec{R}$ is either the summation of normal vectors (0 º < θ < 30 º) or subtraction of them (150 º < θ < 180 º). Two types of parallel stacked arrangements can be distinguished through α-angle; if the α-angle < 45 º, the plane arrangement is considered face-to-face, and if the deviation is > 45 degrees, the arrangement is considered offset stacked. Figure 5 exhibits two scenarios in which the θ-angle < 30 º, and the α-angle is either < 45 º (Figure 5, left) or > 45 º (Figure 5, right). In Figure 5, the black dash line is $\overrightarrow{AB}$ and the red arrow is $\vec{R}$. Table 2 summarizes the criteria to differentiate the types of binding arrangements.

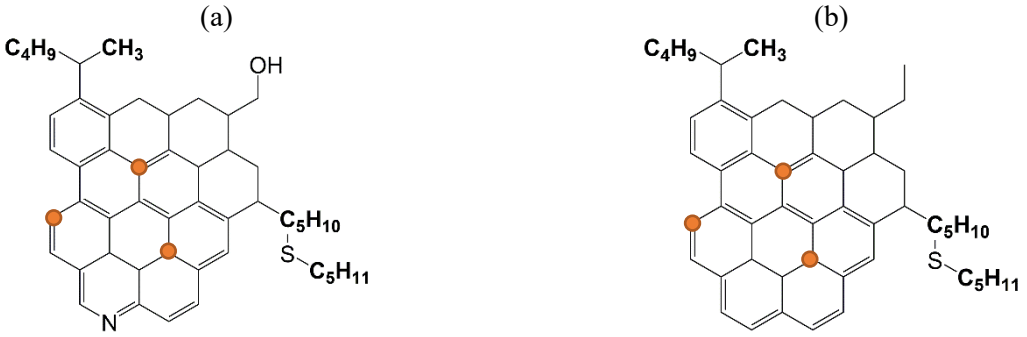

Figure 3. Orange filled circles in panels (a) A2 and (b) A3 show the selected atoms to describe polyaromaic plane in the analysis.

Therefore, using defined parameters and criteria, three types of analysis are conducted in this study. One analysis plots the probability of the θ-angles regardless of the distance between the molecules for the final 60 ns of simulation. The second analysis illustrates the number of intermolecular contact for each binding type along the simulation time for intermolecular COM distance < 1.2 nm. The last plot demonstrates the cumulative number of intermolecular contacts between the molecules for each binding type versus the simulation time in different ranges of molecular COM distance.

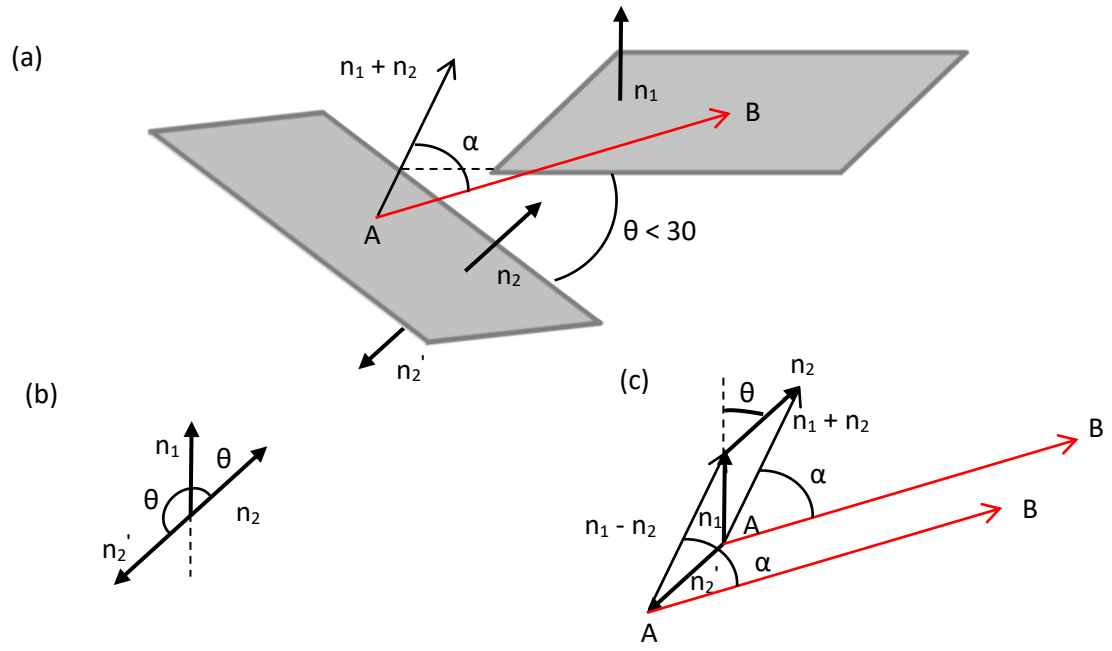

Figure 4: The angle between two planes: (a) the θ- and α-angle between two planes with normal of n_1 and n_2, (b) the θ-angle for co-current and counter-current planes' normal, and (c) the α-angle for both cases of having planes with co-current and counter-current normals.

Table 2. Summarize the criteria to differentiate the binding arrangement.

Distance [nm]	Teta [°]	Alpha [°]	Type
COM < 1.2	$\theta < 30$ or $\theta > 150$	$\alpha < 45$	face-to-face
		$\alpha > 45$	offset stacking
COM < 1.2	$60 < \theta < 120$	not important	T-shape

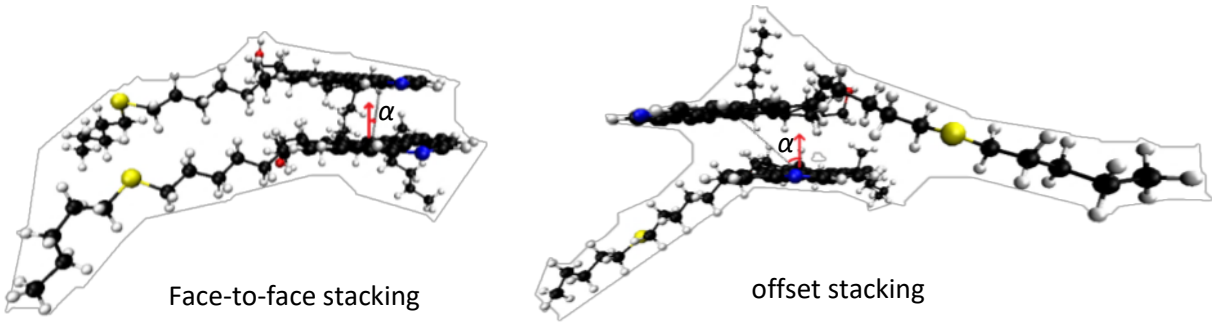

Figure 5: Example of asphaltene arrangements for parallel stacking and offset stacking.

3. RESULTS AND DISCUSSION

3.1. Repeatability of MD Tests

Having reliable and accurate results in both experimental and simulation studies is important. The density of nC_7 at 300K and 1 bar is 678.03 kg/m^3 based on the NIST experimental database [52]. Based on our simulation, the calculated density for A2/nC_7 box reaches 698.14 kg/m^3 (Figure 2), which is justified having 7 wt% asphaltene in the system. Comparing these results verifies the reliability of our simulation. To confirm the repeatability of our simulations, we repeat A3/ nC_7 system three times and compare the aggregate shape characteristics among the replicates. Figure 6 shows the probability distribution of the average aggregate asphericity index for A3/nC_7. Data Set2 shows a lower probability at the peak than data Set 1, while data Set3 indicates the highest probability at the peak, showing a more uniform shape. All three sets are unimodal with a peak at 0.15–0.18 with variation in the y-direction, which means the aggregate shapes are similar, and only the probability of its occurrence has changed. The reason behind the probability difference is that the molecules are initially randomly distributed which can move in different trajectories based on the imposed forces from other molecules but will eventually form similar aggregate shapes. This means that regardless of the random molecule distribution and various movements, the molecule's position and trajectory (as the main simulations output) are similar for the three simulations. Thus, the consistency among replicated MD simulation runs makes our conclusions more reliable. The statistical analysis also shows the similarity between the three simulations as the averages of asphericity for simulation runs 1–3 are 0.189 ± 0.052, 0.209 ± 0.068, and 0.174 ± 0.044.

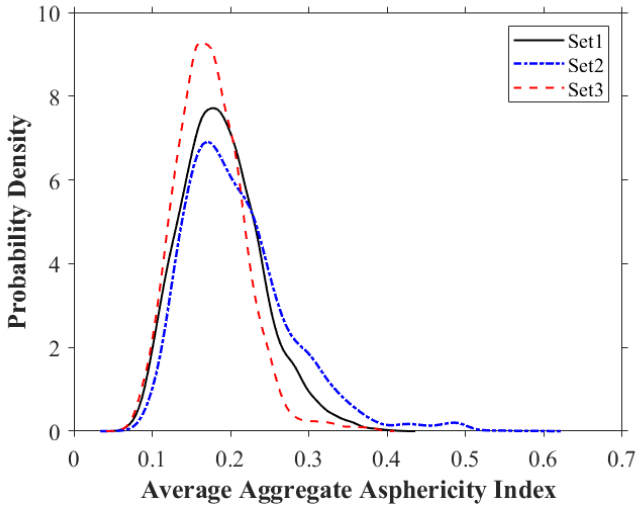

Figure 6: The A3/nC_7 simulation replication shows by analyzing the aggregate shape in the last 60 ns of the simulations.

3.2. Asphaltene Aggregate Shape Using Different Inhibitors

This section discusses the asphaltene aggregation shape for four different asphaltene systems with and without inhibitors. In the first system, 7 wt% of asphaltene is randomly distributed in nC_7, without any inhibitor. In the other three systems, 7 wt% of one inhibitor type, either OP, [BMIM][Br] or [BMIM][Cl], is distributed in the system in addition to the asphaltene/nC_7. We use RDF, angular probability density (θ-angle), and aggregate shape index analyses to study the asphaltene aggregation behavior. In the first two analyses, the arrangements of every two asphaltene molecules are analyzed, using their distance and angle, respectively. The third analysis is based on the aggregate shape, which varies from zero for spherical aggregates to one for rod-like aggregates.

Figure 8 shows the RDF, θ-angle probability density, and the aggregate shape index for A2 asphaltene in the last 60 ns of the simulation. A close look at Figure 8(a) reveals that OP is not able to manipulate the asphaltene interactions within a short distance, whereas [BMIM][Cl] and [BMIM][Br] strongly decrease the $g(r)$ peak at 0.5 nm, which is known as a sign of face-to-face arrangement. The [BMIM][Cl] decreases $g(r)$ peak between 1 and 1.2 nm substantially, which is a sign of the T-shape arrangement. Therefore, based on the RDF plot, all three inhibitors reduce the asphaltene aggregation for pairs of asphaltenes such that the ILs of [BMIM][Cl] and [BMIM][Br] lower both the parallel and T-shape stacking for A2, while OP is more effective at long distance interactions. Figure 8(b) shows the θ-angle probability density between the polyaromatic cores of the asphaltene pairs regardless of their distances with and without the inhibitors. All inhibitors decrease the probability of the asphaltene pairs with an angle range of 60 º–120 º, which is a sign of T-shape arrangement. According to Figure 8(b), OP and [BMIM][Cl] have similar impacts on the asphaltene aggregation, which agrees with the RDF results (Figure 8(a)). Figure 8(c) shows the probability of the aggregate shape index shifting toward higher values (more rod-shape) using inhibitors with a larger distribution. This implies that the inhibitors prevent the aggregation, and smaller aggregates will form more rod-like shapes compared to the inhibitor-free case, in which the aggregates are more uniform and spherical. For instance, Figure 7(a) shows that in general, the asphaltene aggregation is reduced to dimer and trimer aggregates, and asphaltene aggregation has become more relaxed when [BMIM][Cl] is in the system compared with the inhibitor-free case. It also demonstrates that aggregates become smaller with diverse shapes toward more rod-like while there is one large spherical shape without inhibitors (Figure 7(b)). In addition, the shape changes using OP and [BMIM][Cl] inhibitors are similar and in agreement with the angle distribution function (Figure 8(b)), while [BMIM][Br] drastically alters the aggregate asphericity, which is in agreement with the RDF graph (Figure 8 (a)). The RDF analysis does not include angles, and the distance is not considered in angle distribution analysis. Hence, it is challenging to elaborate on the binding arrangement and to relate the binding arrangement to the aggregate shape. For example, the ILs reduce the face-to-face stacking based on the RDF analysis, which only considers the parallel arrangements within short distances. However, the parallel arrangement does not change appreciably based on the angle distribution density, which implies that the long-distance parallel arrangement is increased. Moreover, the RDF analysis and angle distribution density can not discreminat between face-to-face and offset stacking. Therefore, it is necessary to incorporate distance and angle factors to classify the binding arrangements while studying the inhibitor impact.

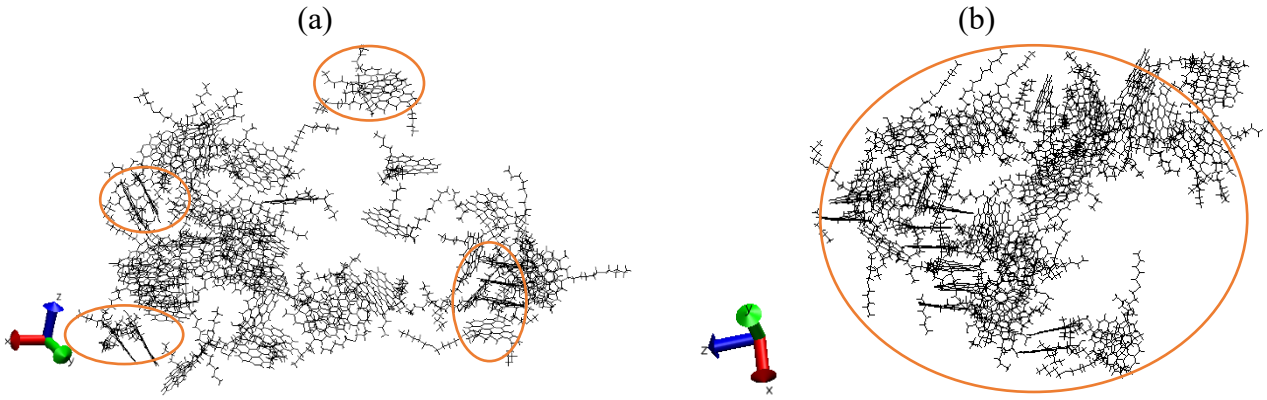

Figure 7. Final A2 molecules arrangement (a) in the presence of [BMIM][Cl] and (b) in the absence of inhibitor. nC_7 and inhibitors are not shown for clarity.

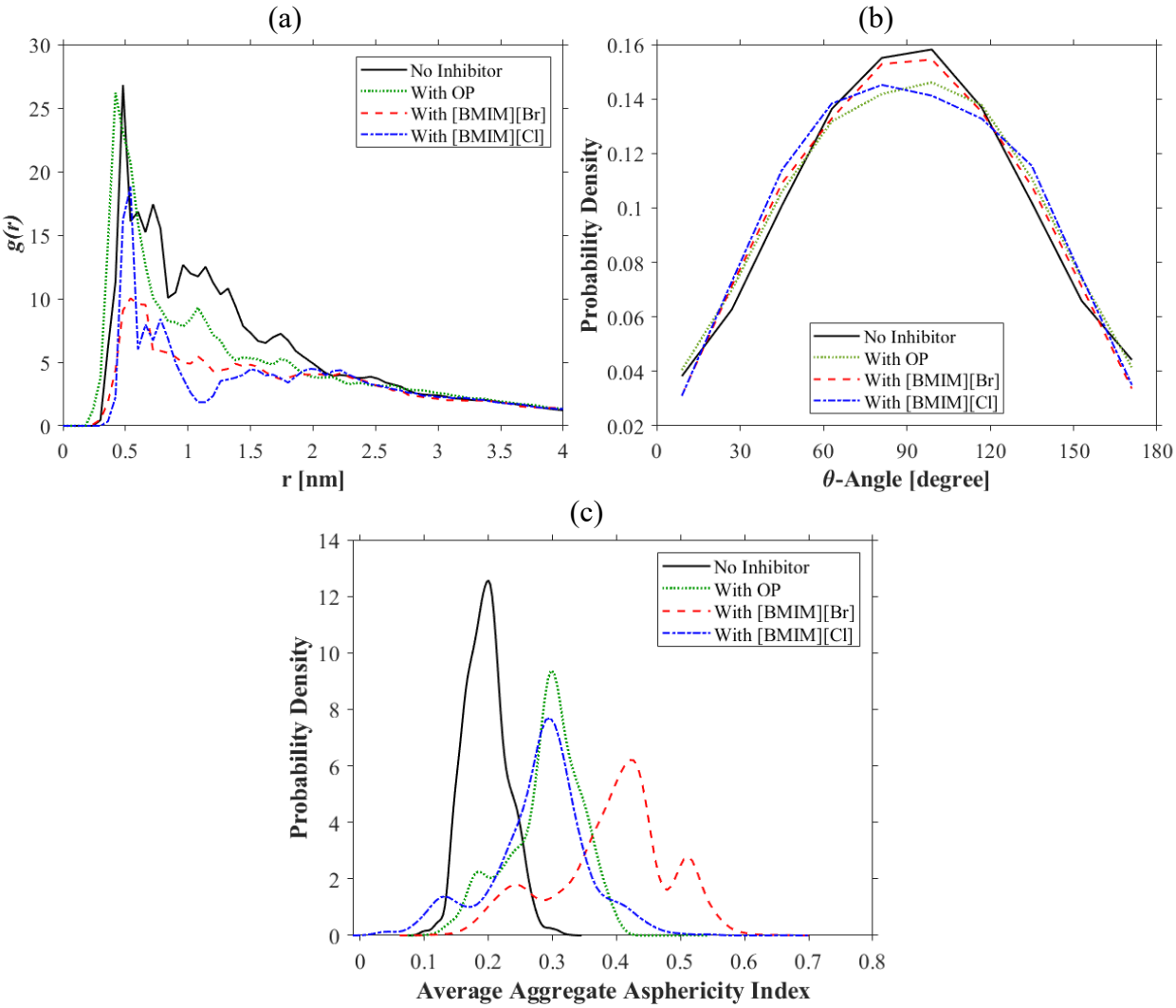

Figure 8: (a) radial distribution function, (b) θ-angle probability density, (c) asphericity index probability density for A2/nC$_7$ without and with inhibitors for final 60 ns simulation run time.

Figure 9 shows the binary arrangements and the asphericity index for A3 at the final 60 ns of the simulation with and without the inhibitors. Based on Figure 9(a), the addition of OP does not significantly change the RDF profiles, while [BMIM][Cl] and [BMIM][Br], respectively, reduce the intensity of $g(r)$ peak at 0.5 nm, which means less face-to-face stacking occurs. Figure 9(b) confirms the reduction of parallel stacking with ILs because the probability of θ-angle in the range 0 º–30 º and 150 º–180 º is less than the case of asphaltene without the inhibitors. The addition of [BMIM][Br] and OP increases and decreases the probability of θ-angles between 60 º–120 º, respectively. These behaviors can dictate the aggregate shape to become more spherical using [BMIM][Br] and more rod-like using OP inhibitors. Figure 9(c) confirms the prediction for asphaltene aggregate shape using [BMIM][Br] and OP inhibitors. The inhibitor-free system has a strong single peak at an asphericity index of 0.2. [BMIM][Br] changes the aggregate shape probability distribution to a bimodal distribution with a higher peak at 0.12, meaning that the aggregates are more spherical than the system without the inhibitor. OP changes the probability distribution to bimodal with peaks shifting the asphericity index to 0.25 and 0.32; this shifting implies that the aggregate shape is altering to rod-like. The asphericity index in the asphaltene system containing [BMIM][Cl] is between the OP and [BMIM][Br] effects. The asphericity

probability distribution using [BMIM][Cl] inhibitor is unimodal, and it is slightly shifted from the case without inhibitor towards rod-like aggregates, which is not noticed in RDF or angle distribution density plots. Again, the misinterpretation and lack of conclusiveness in the RDF and angle distribution density graph highlight the necessity of distance and angle coupling to study the aggregation interaction, which will be discussed in the next sections.

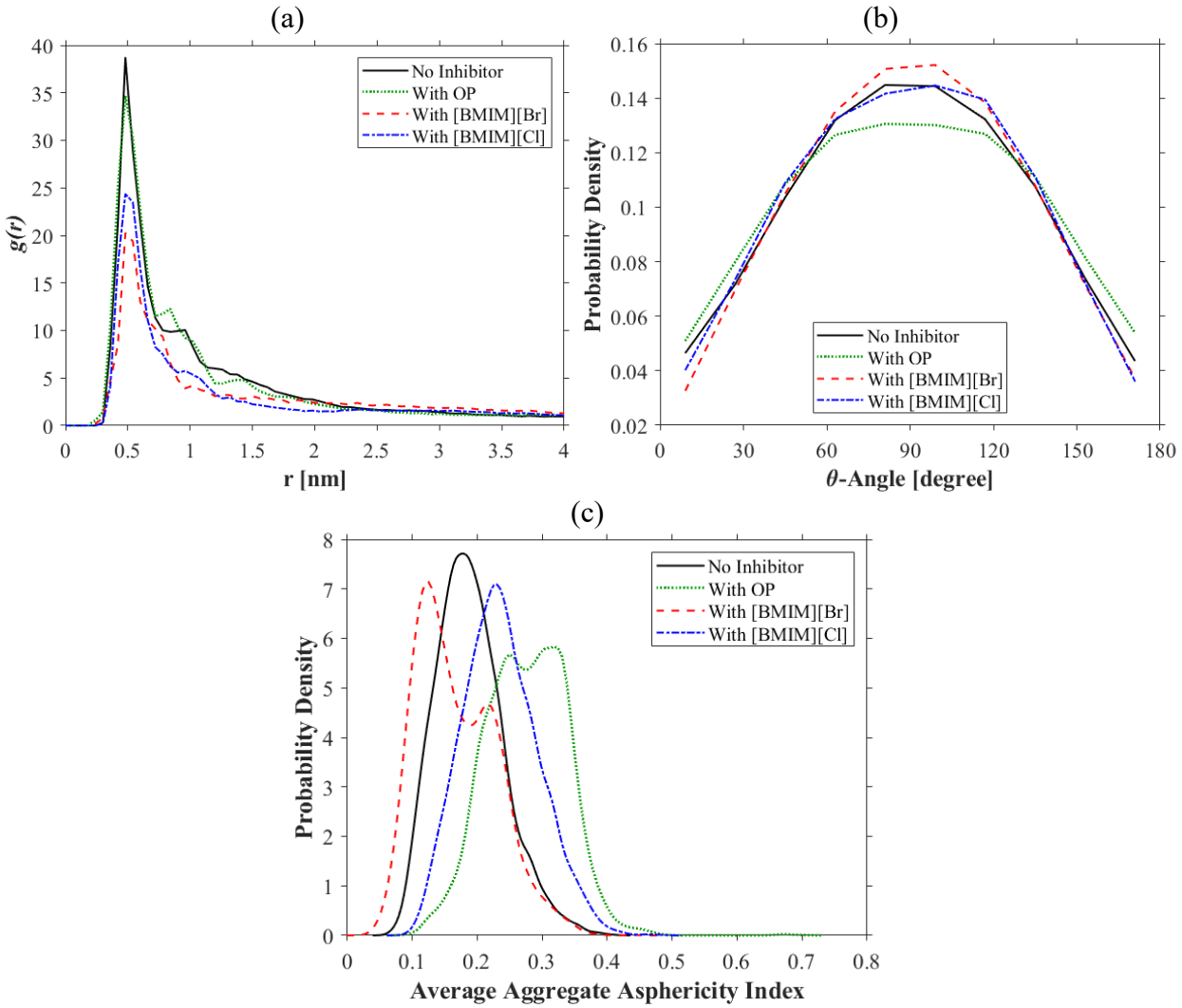

Figure 9: (a) radial distribution function, (b) θ-angle probability density, and (c) asphericity index probability density for A3/nC$_7$ without and with inhibitors for last 60 ns.

3.3. Effect of Inhibitors on the Asphaltene Binding Mechanisms

Asphaltene aggregation has three main binding arrangements: face-to-face, offset stacked, and T-shape stacked. In most research studies in the literature, the center of mass (COM) distance is used to distinguish the aggregation types. However, we believe that considering only distance may result in a false conclusion. For example, identifying the T-shape arrangement mistakenly, rather than offset stacked, if the displacement is large enough that the distance between the molecules' COM falls into the T-shape category. Additionally, an offset stacked arrangement might be misidentified as face-to-face if there is an arrangement with the distance between the COM less than 0.5 nm. Furthermore, the angle between two molecules alone can not be used as an independent variable to differentiate the

aggregation's arrangements, as mentioned in section 3.2. Therefore, we propose considering the distance between the molecules' COM, the angle between two asphaltene polyaromatic cores (θ), and the angle between the vector connecting the centre of polyaromatic cores and the resultant vector of polyaromatic plane normals (α).

Figure 10 displays the number of intermolecular contacts between the asphaltene molecules versus time for the systems without inhibitor (Figure 10 (a)) and with inhibitors (Figure 10 (b)-(d)) when the distance between molecules' COM is < 1.2 nm. The cut-off threshold of 1.2 nm is chosen because the vdW and Coulombic energy contributions are neglected beyond this cut-off distance in the simulation. Also, this value is the maximum limit used for distinguishing the binding arrangement [32]. Figure 10(a) reveals that the face-to-face and T-shape are two main arrangements for A2 binding, and the offset stacked has the minimum contribution to asphaltene binding without an inhibitor. The system containing OP follows a similar order, while the T-shape contribution being significantly lower than the face-to-face such that the face-to-face arrangement is the primary binding mechanism (Figure 10(b)). The fact that OP prevents asphaltene from forming hydrogen bonding (T-shape) derives asphaltenes to form more face-to-face binding, which is also demonstrated in Figure 11. Using [BMIM][Br], face-to-face is the most probable, and the offset stacked is the least probable arrangement for the asphaltene binding, similar to the case with OP and the case without any inhibitor. However, the number of intermolecular contacts for face-to-face drops significantly from 40–45 to 16 (three times) at 120 ns using [BMIM][Br] compared to the cases with no inhibitor and OP (Figure 10(c)). The reduction of face-to-face intermolecular contacts vanishes the dominancy of face-to-face arrangement, and no arrangement is dominant when [BMIM][Br] is added. In contrast, using [BMIM][Cl] as the inhibitor, the number of intermolecular contacts for the face-to-face arrangement is 20, and this mechanism dominates the asphaltene aggregation behavior. Figure 10(d) demonstrates that adding [BMIM][Cl] decreases both the face-to-face and T-shape binding arrangements significantly compared to an inhibitor-free system. The offset stacked and T-shape arrangements have similar ranges of fluctuations with an average value of 5 contacts at 120 ns.

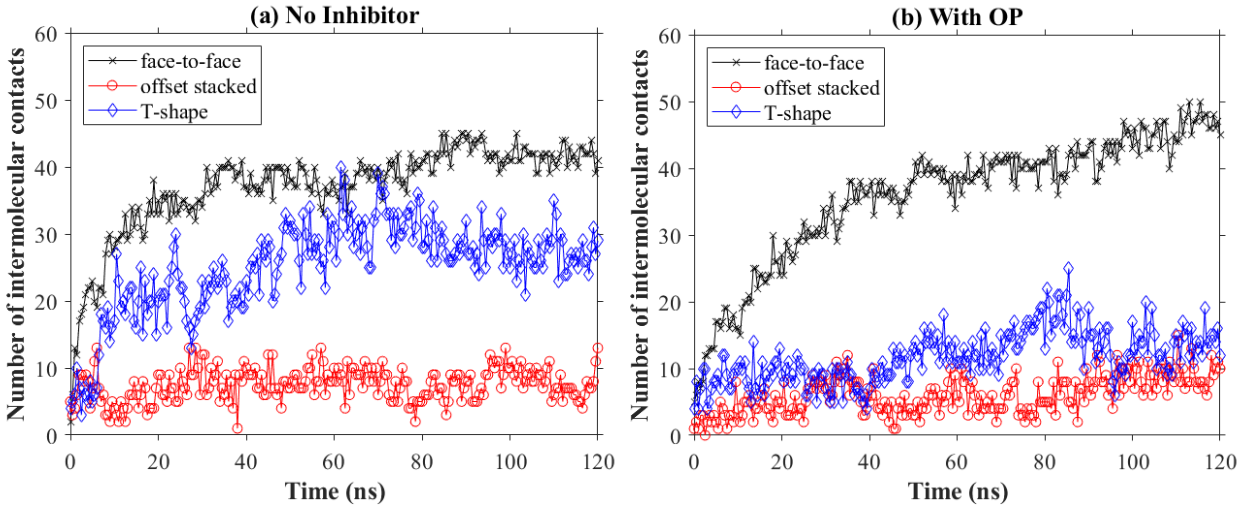

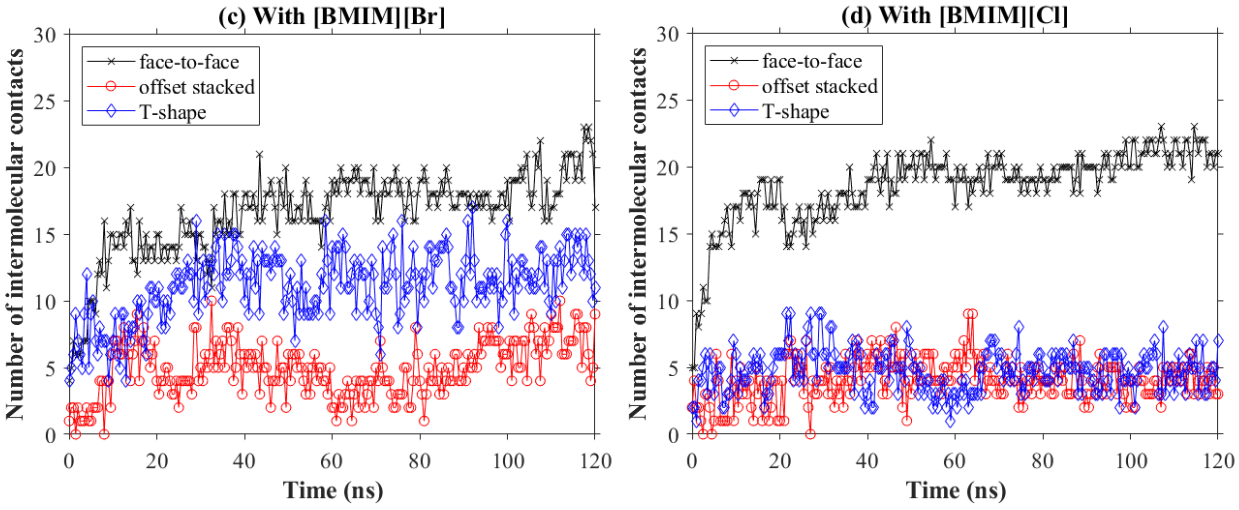

Figure 10: The number of intermolecular contacts for A2/nC_7: (a) no inhibitor, (b) OP addition, (c) [BMIM][Br] addition, and (d) [BMIM][Cl] addition.

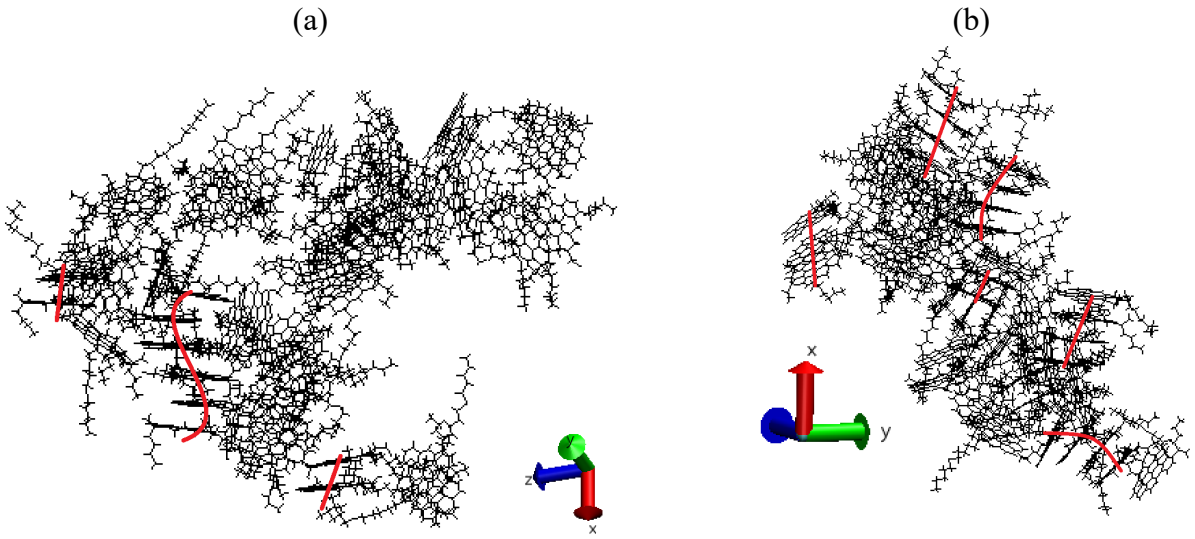

Figure 11. Final A2 molecules arrangement (a) in the absence of inhibitor and (b) in the presence of OP. nC_7 and inhibitors are not shown for clarity. Red lines highlight asphaltenes connected through parallel stacking.

Figure 12 shows the number of intermolecular contacts between A3 molecules for the systems without (Figure 12(a)) and with an inhibitor (Figure 12(b)-(d)) when the distance between the molecules' COM is less than 1.2 nm. In the inhibitor-free system, face-to-face has the highest number of contacts, followed by offset stacked and T-shape, as shown in Figure 12(a). Comparing the binding arrangements for A2 and A3 shows that the face-to-face and T-shape are the dominant binding arrangements for A2; for A3, only the face-to-face is the main binding arrangement. Hence, the order of aggregation mechanisms for A3 is slightly different from A2 due to the A2 capability to form hydrogen bonds. According to Figure 12(b), adding OP only increases the number of face-to-face contacts and does not change the offset stacked and T-shape arrangement order. On the contrary, adding the IL inhibitors decrease the number

of face-to-face arrangements to approximately half and reduces the aggregation by offset stacked to a similar occurrence for the T-shape contact.

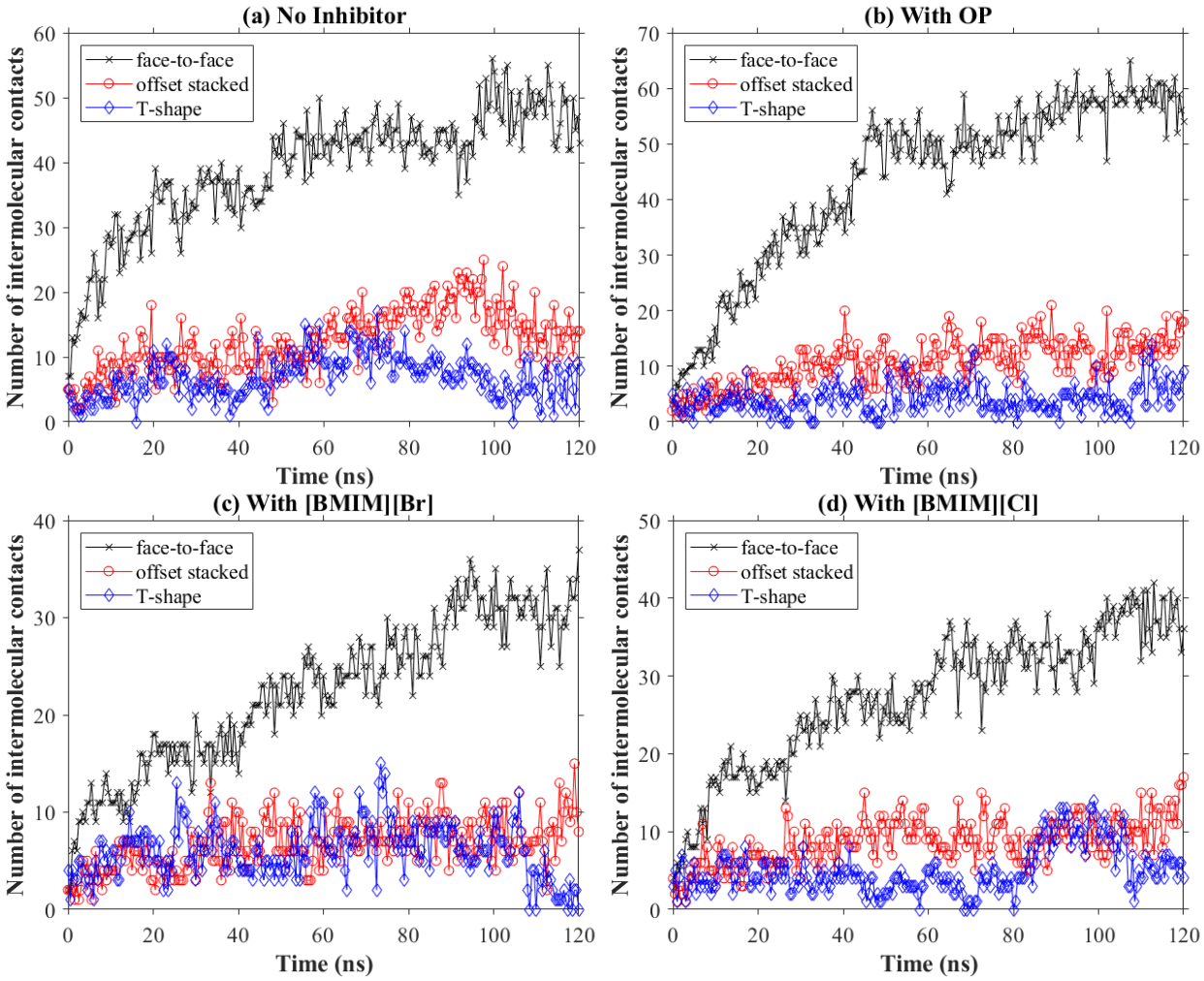

Figure 12: The number of intermolecular contacts for A3/nC$_7$: (a) no inhibitor, (b) OP addition, (c) [BMIM][Br] addition, and (d) [BMIM][Cl] addition.

Therefore, the trend and order of binding arrangements are different for two different asphaltene structures with and without the inhibitors. The binding arrangements are also affected by the type of inhibitor because of the variations in the type of interaction forces for the asphaltene-asphaltene and asphaltene-inhibitors. Gray et al. [5] introduced various forces between the asphaltene molecules based on their chemical structures. The two asphaltene structures employed in this study have quadrupole-quadrupole interaction force, while A2 can form hydrogen bonds. OP has one benzene ring, which is relatively smaller than the asphaltene polyaromatic core with nine aromatic rings. The quadrupole-quadrupole attraction force between the electron cloud in OP and that in the asphaltene polyaromatic is less than the attraction force between the electron clouds of the two polyaromatic cores. Therefore, there is no effective binding between the OP and A3 molecules to stop asphaltene aggregation. Nevertheless, the OP molecules have a hydroxyl group, which results in forming hydrogen bonds with highly electronegative atoms such as oxygen and nitrogen that are available in A2. Therefore, OP forms hydrogen bonding with A2, provides steric effects with the alkyl tail, and reduces the asphaltene binding. Although OP is still incapable of stopping quadrupole-quadrupole interactions between the asphaltene

polyaromatic cores, it prevents the asphaltene molecules from forming hydrogen bonding with themselves and reduces the number of asphaltene T-shape arrangements (Figure 10(b)). ILs are strong electron donor-acceptor that play a crucial role in their inhibitory effect. The IL inhibitor and asphaltene interaction forces are dispersive, hydrogen bond, charge transfer, dipolar, and Coulombic [53]. One of the main interactions between the asphaltene and IL is the cation-quadrupole interaction, which is stronger than the quadrupole-quadrupole interaction. The cation-quadrupole interactions increase if the anion part of the ILs acts as an electron donor, interacting with the electron cloud of the asphaltene polyaromatic core. This mechanism significantly reduces the number of face-to-face contacts for both asphaltenes in the presence of ILs. The anion electron donation capacity is directly related to the anion charge density, which increases by increasing the anion charge and decreasing the anion radius. Chloride has a higher anion charge density than bromide because of its smaller anion size with a similar charge. While both ILs similarly affect the face-to-face binding arrangement for both asphaltenes, [BMIM][Cl] reduces the T-shape binding more for A2, because of its higher electron charge density (as an electron donor).

3.4. Inhibitors' Effect on the Asphaltene Stacking Model

This section discusses the arrangement types within three distance ranges, including 0–0.5 nm, 0.5–0.75 nm, and 0.75–1.2 nm when asphaltenes aggregate with and without inhibitors. This analysis shows the possibility of occurring different stacking models at the above-mentioned distance ranges. Because the number of intermolecular contacts of different arrangements was similar in some cases, the cumulative number of intermolecular contacts is measured and plotted rather than the number of intermolecular contacts in this section.

Figure 13 shows the binding arrangements for A2 with different inhibitors where the COM distance is < 0.5 nm. Although both face-to-face and offset arrangements are observed for all scenarios, T-shape arrangement is not observed due to the lack of space for molecule rotation at this distance. Figure 13(a) shows that the cumulative number of face-to-face arrangements is increased with a steep slope in when adding inhibitor, which implies that the OP promotes face-to-face arrangements within short COM distances. A similar impact is noticed for the offset stacked arrangement, while the OP effect is delayed to the final 20 ns of the simulation (Figure 13(b)). ILs show their significant impacts by reducing the parallel binding at short distances with a more reduction when [BMIM][Br] is used (Figure 13(a)-(b)).

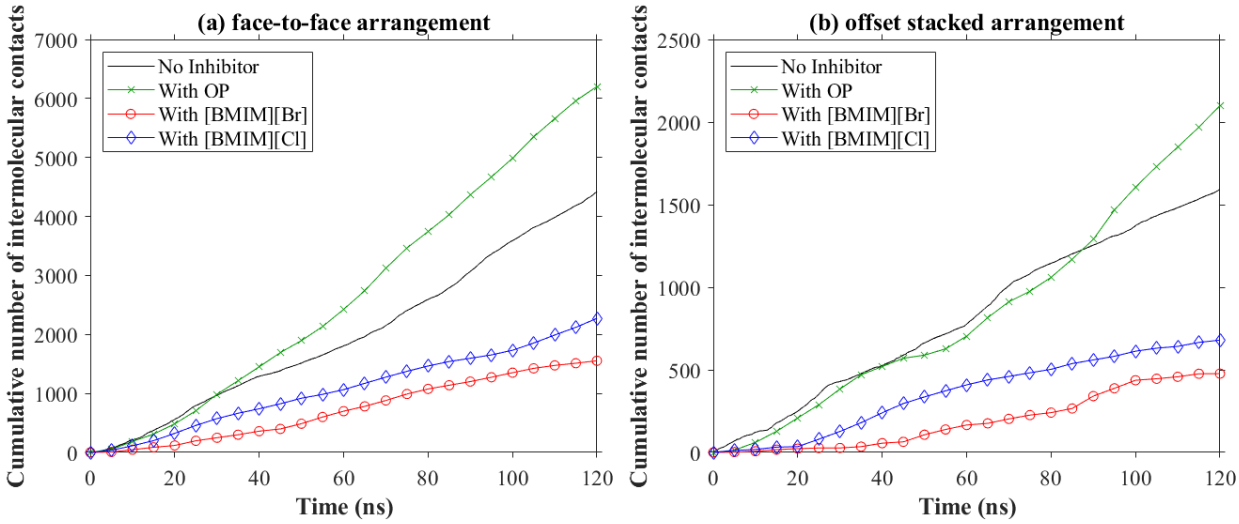

Figure 13: The parallel stacking arrangement for A2/nC_7 in the COM distance range of less than 0.5 nm: (a) face-to-face arrangement and (b) offset stacked arrangement.

Figure 14 shows the A2 binding arrangement in the distance range of 0.5 to 0.75 nm. In this distance range, the face-to-face arrangement is reduced when an inhibitor is added compared to the inhibitor-free system. Figure 14(a) illustrates that the cumulative number of interaction contacts for the face-to-face arrangement decreases in the following order: the inhibitor-free system (the highest), with OP, with [BMIM][Cl], and with [BMIM][Br] (the lowest). While [BMIM][Br] does not change the frequency of the offset stacking occurrences (compared to the inhibitor-free system), OP and [BMIM][Cl] decrease the cumulative number of orderly offset stacked arrangements (Figure 14(b)). Based on Figure 14(c) and comparing the behavior in this panel (c) with those in panels (a) and (b), it can be concluded that the T-shape binding arrangement effectively decreases by adding the inhibitors. The reduction of the T-shape arrangement proves that the aggregate shape changes toward rod-like. The significant reductions of both the face-to-face and T-shape asphaltene arrangements using [BMIM][Br] inhibitor result in a wider range of aggregate shapes (section 3.2).

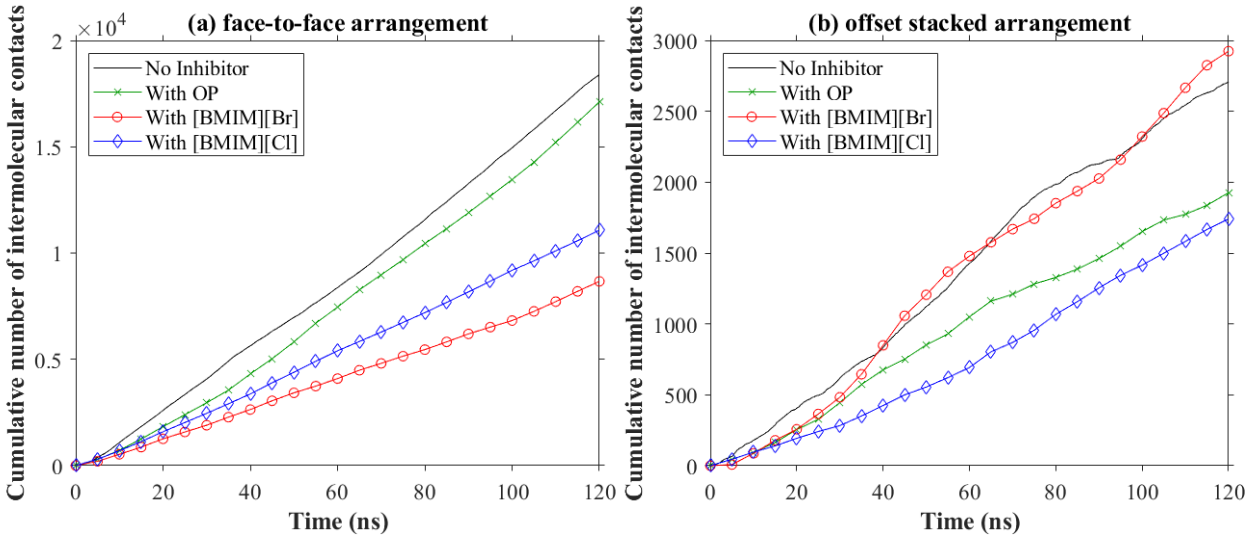

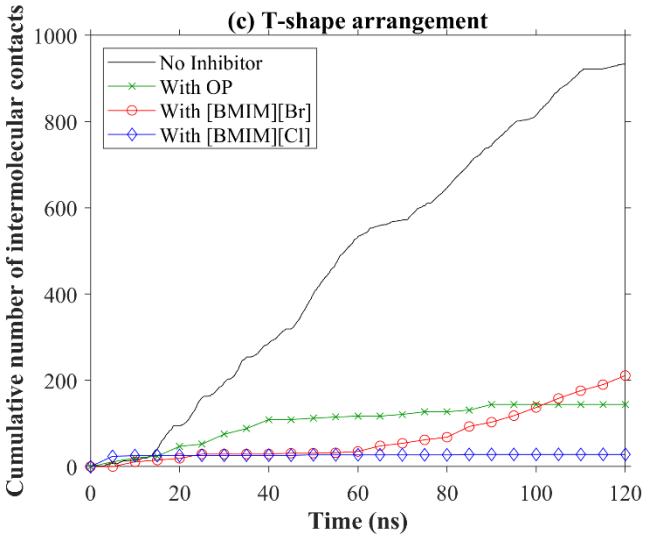

Figure 14: The binding arrangement for A2/nC$_7$ in the COM distance range of 0.5 to 0.75 nm: (a) face-to-face arrangement, (b) offset stacked arrangement, and (c) T-shape arrangement.

Figure 15 shows the asphaltene binding arrangement for A2 when the COM distance range is between 0.75–1.2 nm. For the face-to-face and offset stacked arrangements, the trends and order of the interaction contact number are similar to the 0.5–0.75 nm distance range, except that [BMIM][Br] also reduces the offset stacked arrangement (Figure 15(a)-(b)). Although the ILs eliminate the T-shape binding arrangement for asphaltenes at this distance range, there is a relatively greater extent of T-shape arrangements when using OP (Figure 15(c)). Comparing the T-shape arrangement for OP in the distance range of 0.5–0.75 nm with that in the range of 0.75–1.2 nm reveals that OP controls the asphaltene T-shape binding mostly at lower distances.

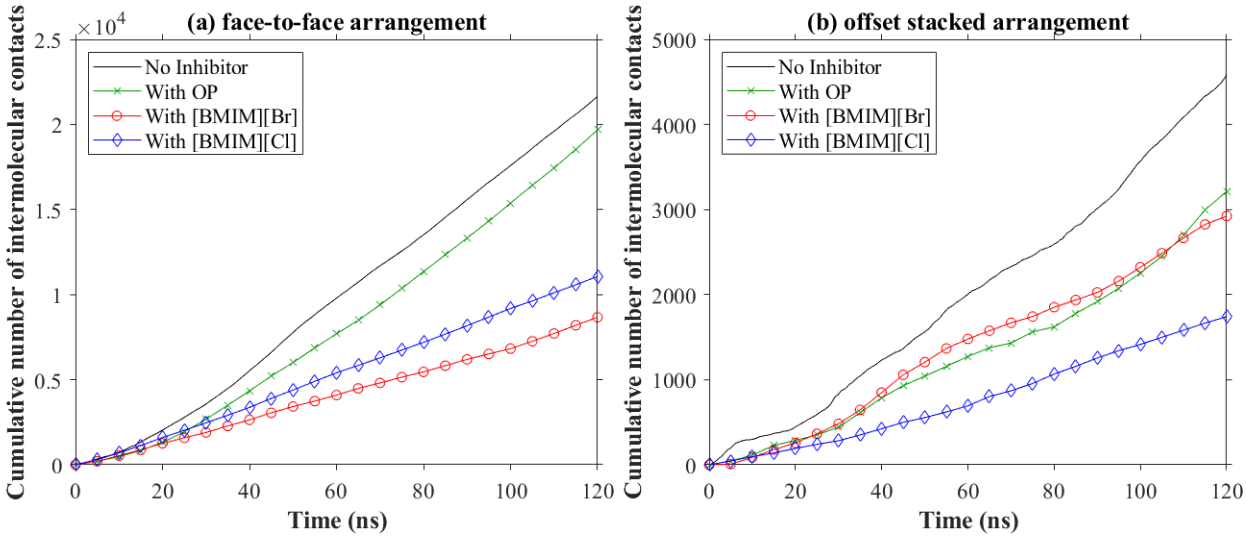

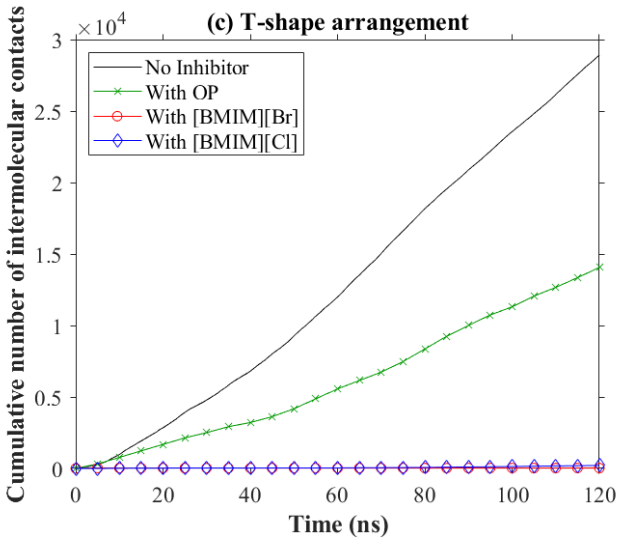

Figure 15: The binding arrangement for A2/nC$_7$ in the COM distance range of 0.75 to 1.2 nm: (a) face-to-face arrangement, (b) offset stacked arrangement, and (c) T-shape arrangement.

4. CONCLUSIONS

The asphaltene molecules bind together through three different coordination arrangements: face-to-face, offset stacked, and T-shape. Usually, the distance between the molecules' centre of mass (COM) is used to discreminate different binding arrangements; using only this feature can sometime result in a false conclusion. We propose an improved framework to differentiate between the binding arrangements by including two angular criteria besides the COM. The angular criteria include the angle between the polyaromatic cores of two molecules and the angle between a vector connecting the centres of polyaromatic cores and resultant vector of plane normals ($\vec{R}$). This method avoids false identification of the binding arrangements for face-to-face stacking with a long separation distance (sandwich arrangement) or for confusing offset stacked with T-shape arrangement. In this study, the effects of *n*-octylphenol (OP) and two IL inhibitors, including 1-butyl-3-methylimidazolium bromide [BMIM][Br], and 1-butyl-3-methylimidazolium chloride [BMIM][Cl] are investigated on the binding arrangements and shape for two different asphaltene structures. The A2 asphaltene has hydroxyl and pyridine groups, while A3 asphaltene does not have either of them. The results imply that OP and [BMIM][Cl] have similar impacts on the aggregate shape for both asphaltenes. However, [BMIM][Br] increases the variations in the aggregate shape for A2 with more probability of forming rod-like aggregates while making the A3 aggregates more spherical. The differences in the behavior of asphaltenes and inhibitors are related to their chemical structure differences, such as the presence of functional groups that result in the interplay between competitive intermolecular forces between the asphaltenes and asphaltene-inhibitors. For instance, the primary inhibitory mechanism of OP is through forming hydrogen bonds with the asphaltene molecules, followed by preventing the growth of asphaltene aggregate. However, OP does not reduce nor prevent quadrupole-quadrupole force between the asphaltene polyaromatic cores. In contrast, ILs cause cation-quadrupole interactions with polyaromatic cores, which is stronger than quadrupole-quadrupole force. Therefore, ILs reduce the number of parallel bindings (especially face-to-face) between the asphaltene molecules. It is also confirmed that the inhibitors have different impacts on asphaltene binding mechanisms at different distance ranges. We expect our results to provide and improve a scientific framework to design and synthesize more effective asphaltene inhibitors under production conditions. For follow-up studies, we recommend considering the effect of asphaltene

deposition on various surfaces (in terms of type, morphology, and composition) in the presence of chemical inhibitors.

References

[1] Teklebrhan RB, Jian C, Choi P, Xu Z, Sjöblom J. Role of naphthenic acids in controlling self-aggregation of a polyaromatic compound in toluene. The Journal of Physical Chemistry B 2016;120(14):3516-26.

[2] Allenson SJ, Walsh MA. A novel way to treat asphaltene deposition problems found in oil production. *International Symposium on Oilfield Chemistry.* Society of Petroleum Engineers; 1997.

[3] Schantz S, Stephenson W. Asphaltene deposition: development and application of polymeric asphaltene dispersants. *SPE Annual Technical Conference and Exhibition.* Society of Petroleum Engineers; 1991.

[4] Sedghi M, Goual L, Welch W, Kubelka J. Effect of asphaltene structure on association and aggregation using molecular dynamics. The Journal of Physical Chemistry B 2013;117(18):5765-76.

[5] Gray MR, Tykwinski RR, Stryker JM, Tan X. Supramolecular assembly model for aggregation of petroleum asphaltenes. Energy & Fuels 2011;25(7):3125-34.

[6] Jian C, Tang T, Bhattacharjee S. Probing the effect of side-chain length on the aggregation of a model asphaltene using molecular dynamics simulations. Energy & fuels 2013;27(4):2057-67.

[7] Murgich J. Intermolecular forces in aggregates of asphaltenes and resins. Petroleum science and technology 2002;20(9-10):983-97.

[8] Chang C-L, Fogler HS. Stabilization of asphaltenes in aliphatic solvents using alkylbenzene-derived amphiphiles. 1. Effect of the chemical structure of amphiphiles on asphaltene stabilization. Langmuir 1994;10(6):1749-57.

[9] Javanbakht G, Sedghi M, Welch WR, Goual L, Hoepfner MP. Molecular polydispersity improves prediction of asphaltene aggregation. Journal of Molecular Liquids 2018;256:382-94.

[10] Gao F, Xu Z, Liu G, Yuan S. Molecular dynamics simulation: the behavior of asphaltene in crude oil and at the oil/water interface. Energy & fuels 2014;28(12):7368-76.

[11] Sodero AC, Santos Silva H, Guevara Level P, Bouyssiere B, Korb J-P, Carrier H, et al. Investigation of the effect of sulfur heteroatom on asphaltene aggregation. Energy & Fuels 2016;30(6):4758-66.

[12] Pacheco-Sánchez J, Zaragoza I, Martínez-Magadán J. Asphaltene aggregation under vacuum at different temperatures by molecular dynamics. Energy & fuels 2003;17(5):1346-55.

[13] Hunter CA, Sanders JK. The nature of. pi.-. pi. interactions. Journal of the American Chemical Society 1990;112(14):5525-34.

[14] Boek ES, Yakovlev DS, Headen TF. Quantitative molecular representation of asphaltenes and molecular dynamics simulation of their aggregation. Energy & Fuels 2009;23(3):1209-19.

[15] Narten A. X-ray diffraction pattern and models of liquid benzene. The Journal of Chemical Physics 1977;67(5):2102-8.

[16] Evans D, Watts R. On the structure of liquid benzene. Molecular Physics 1976;32(1):93-100.

[17] Alvarez-Ramirez F, Ramirez-Jaramillo E, Ruiz-Morales Y. Calculation of the interaction potential curve between asphaltene− asphaltene, asphaltene− resin, and resin− resin systems using density functional theory. Energy & Fuels 2006;20(1):195-204.

[18] Headen TF, Boek ES, Skipper NT. Evidence for asphaltene nanoaggregation in toluene and heptane from molecular dynamics simulations. Energy & Fuels 2009;23(3):1220-9.

[19] Zhang L, Greenfield ML. Molecular orientation in model asphalts using molecular simulation. Energy & fuels 2007;21(2):1102-11.
[20] Rodríuez J, Sánchez-Marín J, Torrens F, Ruette F. Molecular aggregation of polycyclic aromatic hydrocarbons. A theoretical modelling of coronene aggregation. Journal of Molecular Structure: THEOCHEM 1992;254:429-41.
[21] Mullins OC, Sheu EY. Structures and dynamics of asphaltenes. Springer Science & Business Media; 2013.
[22] Teklebrhan RB, Ge L, Bhattacharjee S, Xu Z, Sjöblom J. Probing structure–nanoaggregation relations of polyaromatic surfactants: a molecular dynamics simulation and dynamic light scattering study. The Journal of Physical Chemistry B 2012;116(20):5907-18.
[23] Wang W, Taylor C, Hu H, Humphries KL, Jaini A, Kitimet M, et al. Nanoaggregates of diverse asphaltenes by mass spectrometry and molecular dynamics. Energy & Fuels 2017;31(9):9140-51.
[24] Jian C, Tang T. One-dimensional self-assembly of polyaromatic compounds revealed by molecular dynamics simulations. The Journal of Physical Chemistry B 2014;118(44):12772-80.
[25] Shi M-M, Chen Y, Nan Y-X, Ling J, Zuo L-J, Qiu W-M, et al. π− π interaction among violanthrone molecules: Observation, enhancement, and resulting charge transport properties. The Journal of Physical Chemistry B 2011;115(4):618-23.
[26] Pacheco-Sánchez J, Alvarez-Ramirez F, Martínez-Magadán J. Morphology of aggregated asphaltene structural models. Energy & fuels 2004;18(6):1676-86.
[27] Khalaf MH, Mansoori GA. A new insight into asphaltenes aggregation onset at molecular level in crude oil (an MD simulation study). Journal of Petroleum Science and Engineering 2018;162:244-50.
[28] Mikami Y, Liang Y, Matsuoka T, Boek ES. Molecular dynamics simulations of asphaltenes at the oil–water interface: from nanoaggregation to thin-film formation. Energy & Fuels 2013;27(4):1838-45.
[29] Liu J, Zhao Y, Ren S. Molecular dynamics simulation of self-aggregation of asphaltenes at an oil/water interface: formation and destruction of the asphaltene protective film. Energy & Fuels 2015;29(2):1233-42.
[30] Song S, Zhang H, Sun L, Shi J, Cao X, Yuan S. Molecular Dynamics Study on Aggregating Behavior of Asphaltene and Resin in Emulsified Heavy Oil Droplets with Sodium Dodecyl Sulfate. Energy & fuels 2018;32(12):12383-93.
[31] Lv G, Gao F, Liu G, Yuan S. The properties of asphaltene at the oil-water interface: A molecular dynamics simulation. Colloids and Surfaces A: Physicochemical and Engineering Aspects 2017;515:34-40.
[32] Yaseen S, Mansoori GA. Asphaltene aggregation due to waterflooding (A molecular dynamics study). Journal of Petroleum Science and Engineering 2018;170:177-83.
[33] Santos Silva H, Alfarra A, Vallverdu G, Bégué D, Bouyssiere B, Baraille I. Sensitivity of asphaltene aggregation toward the molecular architecture under desalting thermodynamic conditions. Energy & fuels 2017;32(3):2681-92.
[34] He L, Wang P, He L, Qu Z, Luo J, Peng B, et al. Molecular dynamics simulations of the self-organization of side-chain decorated polyaromatic conjugation molecules: phase separated lamellar and columnar structures and dispersion behaviors in toluene solvent. RSC advances 2018;8(20):11134-44.
[35] Bian H, Xu F, Kan A, Wei S, Zhang H, Zhang S, et al. Insight into the mechanism of asphaltene disaggregation by alkylated treatment: An experimental and theoretical investigation. Journal of Molecular Liquids 2021;343:117576.

[36] Ahmadi M, Chen Z. Comprehensive molecular scale modeling of anionic surfactant-asphaltene interactions. Fuel 2021;288:119729.
[37] Rahmati M. Effects of heteroatom and aliphatic chains of asphaltene molecules on their aggregation properties in aromatics Solvents: A molecular dynamics simulation study. Chemical Physics Letters 2021;779:138847.
[38] Du C, Li D, Shi C, Du Z, Han W, Zhu Y, et al. Study on the association driving force of low temperature coal tar asphaltenes. Journal of Molecular Structure 2022;1254:132361.
[39] Xu J, Wang N, Xue S, Zhang H, Zhang J, Xia S, et al. Insights into the mechanism during viscosity reduction process of heavy oil through molecule simulation. Fuel 2022;310:122270.
[40] Zhang H, Liu S, Wang X, Yuan S, Yuan S. Molecular dynamics study on emulsified oil droplets with nonionic surfactants. Journal of Molecular Liquids 2022;346:117102.
[41] Lindahl, Abraham, Hess, & Spoel, V. D. . GROMACS 2019.3 Source code. 2019.
[42] Abraham MJ, Murtola T, Schulz R, Páll S, Smith JC, Hess B, et al. GROMACS: High performance molecular simulations through multi-level parallelism from laptops to supercomputers. SoftwareX 2015;1:19-25.
[43] Fu C-F, Tian SX. A comparative study for molecular dynamics simulations of liquid benzene. Journal of chemical theory and computation 2011;7(7):2240-52.
[44] Ghamartale A, Zendehboudi S, Rezaei N. New Molecular Insights into Aggregation of Pure and Mixed Asphaltenes in the Presence of n-Octylphenol Inhibitor. Energy & Fuels 2020.
[45] El-hoshoudy A, Ghanem A, Desouky S. Imidazolium-based ionic liquids for asphaltene dispersion; experimental and computational studies. Journal of Molecular Liquids 2021;324:114698.
[46] Clarke PF, Pruden BB. Asphaltene precipitation from Cold Lake and Athabasca bitumens. Petroleum science and technology 1998;16(3-4):287-305.
[47] Hanwell MD, Curtis DE, Lonie DC, Vandermeersch T, Zurek E, Hutchison GR. Avogadro: an advanced semantic chemical editor, visualization, and analysis platform. Journal of cheminformatics 2012;4(1):17.
[48] Nosé S. A molecular dynamics method for simulations in the canonical ensemble. Molecular physics 1984;52(2):255-68.
[49] Hoover WG. Canonical dynamics: Equilibrium phase-space distributions. Physical review A 1985;31(3):1695.
[50] Parrinello M, Rahman A. Strain fluctuations and elastic constants. The Journal of Chemical Physics 1982;76(5):2662-6.
[51] Silva HS, Sodero AC, Bouyssiere B, Carrier H, Korb J-P, Alfarra A, et al. Molecular dynamics study of nanoaggregation in asphaltene mixtures: Effects of the N, O, and S heteroatoms. Energy & Fuels 2016;30(7):5656-64.
[52] Lemmon EW. Thermophysical properties of fluid systems. NIST Chemistry WebBook: NIST Standard Reference Database Number 69 1998;20899.
[53] Boukherissa M, Mutelet F, Modarressi A, Dicko A, Dafri D, Rogalski M. Ionic liquids as dispersants of petroleum asphaltenes. Energy & Fuels 2009;23(5):2557-64.